

Quantum chemical characterization of single molecule magnets based on uranium

Mariano Spivak,¹ Konstantinos D. Vogiatzis,^{2,‡} Christopher J. Cramer,^{2} Coen de Graaf,^{1,3} and Laura Gagliardi.^{2*}*

¹Departament de Química Física i Inorgànica, Universitat Rovira i Virgili, Marcel·lí Domingo s/n, E-43007 Tarragona, Spain.

²Department of Chemistry, Chemical Theory Center, and Supercomputing Institute, University of Minnesota, Minneapolis, Minnesota 55455, United States.

³ICREA, Passeig Lluís Companys 23, 08010, Barcelona, Spain.

[‡]Current address: Department of Chemistry, University of Tennessee, Knoxville, Tennessee 37996, United States.

Abstract. Multiconfigurational electronic structure theory calculations including spin-orbit coupling effects were performed on four uranium-based single-molecule-magnets. Several quartet and doublet states were computed and the energy gaps between spin-orbit states were then used to determine magnetic susceptibility curves. Trends in experimental magnetic susceptibility curves were well reproduced by the calculations, and key factors affecting performance were identified.

I. INTRODUCTION

Magnetic materials used in information storage and spin-electronics owe their properties to the spin interactions between neighboring units in the bulk. Molecules containing several transition-metal ions can exhibit properties similar to nanoscale magnetic particles (nanomagnets). Some of these polynuclear clusters possess energetically isolated high-spin ground states in which spin-orbit coupling results in zero-field splitting of the $(2S + 1)$ -fold degenerate ground multiplet. These compounds exhibit slow relaxation of the magnetization of purely molecular origin and are defined as single-molecule magnets, SMMs. An early example was the polynuclear manganese cluster $\text{Mn}_{12}\text{O}_{12}(\text{CH}_3\text{COO})_{16}(\text{H}_2\text{O})_4$,¹ and other manganese compounds have been subsequently reported.² The particular appeal of SMMs is their potential to reduce the length scale of magnetic materials constructed from them when compared to traditional magnets.

There are specific challenges associated with constructing magnetic materials from SMMs. For instance, in transition-metal SMMs the magnetic relaxation blocking temperatures are generally quite low.³ On the other hand, SMMs that contain single and multiple lanthanide ions have large first-order spin-orbit couplings associated with these heavier elements, and this can generate large magnetic anisotropies.⁴ These anisotropies give rise to increased relaxation barriers and therefore decreased (slower) magnetic relaxation.^{4d, 5} However, well-isolated high-spin ground states are difficult to achieve within polynuclear lanthanide SMMs because the valence 4f orbitals have limited radial extent and are usually energetically incompatible with ligand orbitals. These inherent properties of the 4f orbitals result in predominantly ionic interactions between neighboring spin centres which involve only weak magnetic superexchange coupling.^{4a}

Given their still larger spin-orbit coupling and the radial extension of the 5f orbitals, the actinides offer more promise for the design of both mononuclear and exchange-coupled molecules, and actinide SMMs have indeed emerged. By some measures, the actinides are already demonstrating promise.⁶ However, work remains to understand the nature of the slow relaxation in mononuclear actinide complexes, as well as the influence of magnetic exchange on slow relaxation in multinuclear species. With large spin-orbit couplings and potentially strong metal-metal interactions in polynuclear complexes, the actinides uniquely combine the optimal characteristics of the lanthanides and transition metals.

The potential combination of large magnetic anisotropies with covalent character in metal-ligand interactions poses special challenges for both theory and experiment. While covalency is advantageous for generating strong magnetic exchange, it does make the rational design of mononuclear actinide complexes more challenging, and synthetic approaches to actinide compounds tend to be different compared to those for lanthanides or transition-metal complexes.⁶ From the standpoint of modeling, actinide-containing systems have complex electronic structures owing to open-shell 5f orbitals and strong relativistic effects, including especially spin-orbit coupling. Indeed, such molecules are inherently multiconfigurational, i.e., systems whose electronic density matrices cannot be represented to a good approximation by a single Slater determinant or a single configuration-state-function (CSF). Such systems are usually labeled as “strongly correlated” systems or “multireference” systems, where the latter reminds us that a single-reference wave function theory (WFT) model is inadequate and instead a multiconfigurational reference state must be employed to adequately account for the “static” (also sometimes called “nondynamical,” “near-degeneracy,” or “left–right”) correlation energy.⁷

For inherently multiconfigurational systems, Kohn-Sham Density Functional Theory (DFT) faces the intrinsic challenge that it is by construction a single-determinantal model and thus, with currently available functionals, DFT tends to perform with unsystematic accuracy when evaluated over a range of such cases.⁸ By contrast, multiconfigurational self-consistent-field (MCSCF) methods, such as the complete active space self-consistent field (CASSCF)⁹ method, treat near-degeneracies with no ambiguity with respect to the state of interest; however, they do not include dynamical correlation energy (which is associated with the correlated movements of individual electrons at shorter range) that is essential for a quantitative treatment of chemical properties like bond energies and electronic excitation energies. They also do not generally include core-valence correlation, which can be an additional important contributor to the electronic structure of heavy element systems. The energetic consequences of these phenomena *can* be computed via a post-SCF method, for example multireference perturbation theory (e.g., complete-active-space second-order perturbation theory (CASPT2)¹⁰ or multireference configuration interaction (MRCI)¹¹ theory, using the MCSCF reference wave function, but such methods are limited in their applicability systems of small to modest size owing to a computational cost that scales steeply as a function of the increasing size of the system. For large systems in which both static and dynamical correlation energy are crucial, a method that allows a description of both types of correlation with affordable computational costs is needed.

With respect to the CASSCF method, the many-electron wave function has the formally desirable property of being independent of unitary transformations within the spaces of inactive, active, and external orbitals. Modern extensions of CASSCF sacrifice this property by not including *all* possible distributions of active electrons into active orbitals, with the desirable trade-off being that this allows practical access to overall larger active spaces. Examples of

methods employing such incomplete configuration lists are restricted active space SCF (RASSCF),¹² generalized active space SCF (GASSCF),¹³ and occupation-restricted-multiple-active-space SCF (ORMAS).¹⁴ In the RASSCF model,¹² for example, the active orbitals are divided into up to three distinct subspaces, and minimum and maximum electron occupation numbers are applied to two of these subspaces, respectively, thereby substantially reducing the number of determinants that contribute to a given CSF.

For SMM systems, most previous studies have avoided the calculation of a PT2 correction because of its high computational expense,¹⁵ reporting results at the SCF level, instead. Given a limited number of results in the literature to date, it is not yet clear if CASPT2 can serve as a benchmark standard method for systems where the energetic consequence of spin-orbit coupling is of equal or greater magnitude to that of dynamic electron correlation. We here examine this point further by employing different multiconfigurational methods for characterization of the electronic structures of a series of uranium-based SMMs. In particular, we compare different active spaces both in the CASSCF and RASSCF formalism, and we apply corrections from second-order perturbation theory and spin-orbit coupling to obtain excitation energies and magnetic susceptibilities that rationalize trends with respect to structural differences.

We examine specifically $U(H_2Bpz_2)_3$ (**1**; $H_2Bpz_2^-$ = dihydrobis(pyrazolyl)borate),¹⁶ $U(Bp^{Me})_3$ (**2**; Bp^{Me-} = dihydrobis(methylpyrazolyl)borate), $U(Bc^{Me})_3$ (**3**; Bc^{Me-} = dihydrobis(methylimidazolyl)borate),¹⁷ and UTp_3 (**4**; Tp^- = hydrotris(pyrazolyl)borate)¹⁸ (Figure 1). These compounds are among the first experimentally characterized uranium-based SMMs and by spanning a range of related structural motifs, including different coordination numbers and atoms bonded to the metal, they provide an excellent series to better understand how ligand variation affects the magnetic properties of such uranium compounds.

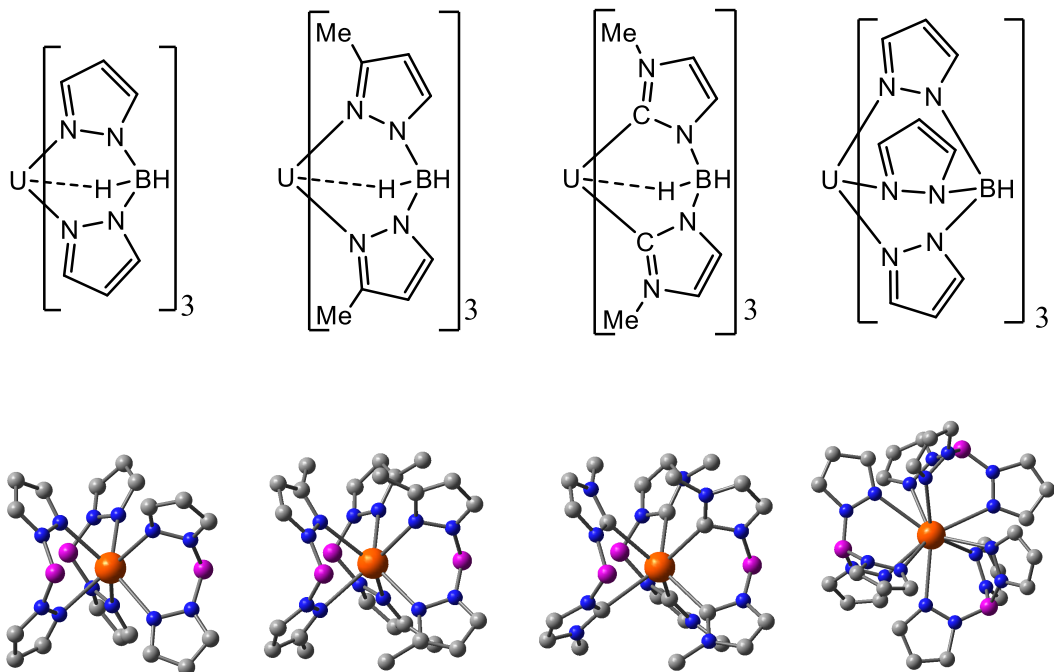


Figure 1: Compounds **1**, **2**, **3** and **4** from left to right. Line drawings (top) and 3D structures (bottom). Color code: orange U, blue N, grey C, purple B. Hydrogen atoms omitted for clarity.

II. COMPUTATIONAL METHODS

Wave functions for all compounds were computed at the complete active space self consistent field (CASSCF)⁹ and restricted active space self consistent field (RASSCF)¹² level of theory as implemented in the MOLCAS 8.0 software package.¹⁹ All-electron basis sets of atomic natural orbital type with relativistic core corrections (ANO-RCC) were used,²⁰ for U with triple-zeta plus polarization quality, TZP, and for the remaining atoms (N, C, B, H) with double-zeta plus polarization quality, DZP. Scalar relativistic effects were included using the Douglas-Kroll-Hess Hamiltonian.²¹ The computational cost of computing the two-electron integrals was reduced by

recourse to the Cholesky decomposition technique (with a cut-off threshold to 10^{-8} a.u.).²² The smallest active space required to account for all possible distributions of three valence electrons (consistent with U(III)) in seven 5f orbitals is CAS(3,7). This active space generates 35 quartet and 112 doublet states. We also examined active space extensions to include occupied orbitals from the π systems of the ligands, thereby encompassing low-energy ligand-to-metal charge-transfer (LMCT) excited states (CAS(7,9) when including two occupied π orbitals). When considering the inclusion of ligand virtual orbitals that would further encompass metal-to-ligand charge-transfer (MLCT) states, we observed that atomic states from U 5f-6d excitations appeared at lower energies. Thus, we constructed a third active space which added the five unoccupied U 6d orbitals using the RASSCF formalism (RAS(3,12)). A RASSCF wave function has fewer CSFs than the corresponding CASSCF wave function and can be defined in such a way to avoid the inclusion of high energy states, such as $5f^06d^3$, that might induce convergence problems in the state average procedure and a poor description of the lowest energy states. Spin-orbit effects were taken into account *a posteriori* with the RAS State Interaction (RASSI) method.²³ In selected instances, subsequent multi-state CASPT2¹⁰ calculations were performed with an imaginary shift of 0.2 atomic units, which reduces instabilities associated with weak intruder states.

Magnetic susceptibility values were computed with the SINGLE-ANISO code,²⁴ which uses the energies (ϵ) and magnetic moment (μ) of the spin-orbit states calculated from RASSI in a formula based on the van Vleck formalism (Equation 1). The magnetic susceptibility arises from a sum over the spin-orbit states (i,j) of their respective magnetic moments ($\mu(i,j)$ is a complex tensor in the basis of the spin-orbit states), each weighted by that state's Boltzmann population at a given temperature.

$$\chi(T) \propto \frac{\sum_i e^{-\frac{\epsilon_i}{kT}} \sum_j \|\mu(i,j)\|^2}{\sum_i e^{-\frac{\epsilon_i}{kT}}} \quad (\text{Eq. 1})$$

Single-crystal X-ray structures have been reported for **1–3**, but not for **4**. To validate a DFT model for use in predicting a geometry for **4**, we optimized the geometry of **1** with the BP86,²⁵ B3LYP²⁶ and M06-L²⁷ functionals using a TZ2P basis set on U, a DZP basis for all other atoms, and the zero order regular approximation (ZORA) to account for scalar relativistic effects.²⁸ As BP86 provided the best agreement with experiment for **1** (Table 1), it was also used to optimize the geometry of **4** for use in subsequent multireference calculations. All DFT calculations were performed with the ADF2013.1 software package.²⁹

Table 1: Comparison of structural parameters for the DFT optimization of compound **1**.

Method	U-N _{pz} (Å)	U-B (Å)	N-U-N (°)
Experimental	2.535	3.278	78.9
BP86	2.528	3.237	80.6
B3LYP	2.558	3.308	77.6
M06-L	2.574	3.283	76.5

III. RESULTS

All of the studied compounds have been experimentally characterized with quartet ($S=3/2$, $^4I_{9/2}$) ground states, as expected for the $5f^3$ configuration of U(III), but many low-lying excited states have also been observed with both quartet and doublet ($S=1/2$) multiplicity.³⁰ Given the potentially significant covalency of bonds involving actinide $5f$ orbitals, ligand to metal charge transfer (LMCT) states can have energies low enough to play a role in spin-orbit coupling. This is true also for states generated by uranium $5f$ to $6d$ excitations ($5f^26d^1$ configuration). Figure 2

provides a summary of the results for compound **1**, with all electronic states classified by their nature. As expected, the $5f^3$ states are the lowest in energy, with the quartet ground state (GS) taken as the relative zero of energy. Both quartet and doublet LMCT states appear about $100,000\text{ cm}^{-1}$ (12.4 eV) above the GS, which suggests little to no spin-orbit interaction between them and the $5f^3$ states. Uranium $5f^26d^1$ states are predicted to be closer in energy, but the energy gap separating them from the U $5f^3$ quartet states is still sizable (more than $15,000\text{ cm}^{-1}$, or about 1.9 eV).

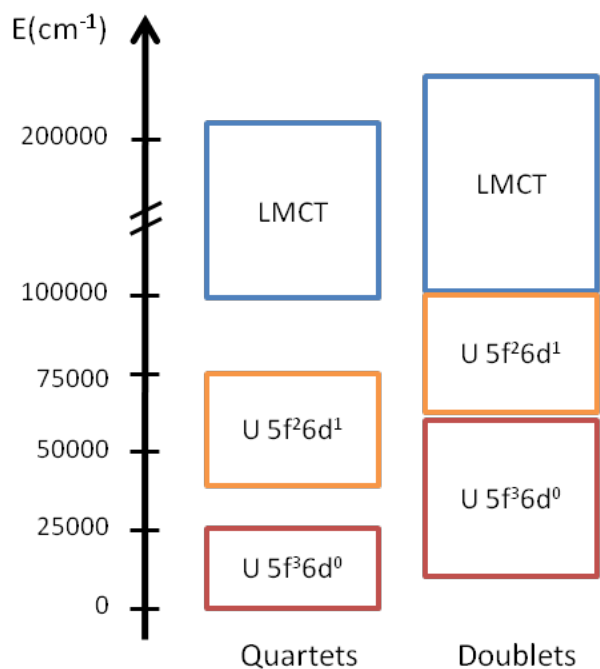


Figure 2: Schematic representation of the CASSCF/RASSCF relative energies for compound **1**.

Given these various state energies, we first computed spin-orbit couplings between the lowest-energy states formed by combining all $5f^3$ and $5f^26d^1$ configurations and using the associated

RASSCF(3,12) energies. Our results indicated no coupling between the two sets of states, with computed spin-orbit state energies invariant to the presence of the $5f^26d^1$ states (Table S9).

On that basis, we conclude that the CAS(3,7) active space is sufficient to encompass all states energetically relevant for spin-orbit coupling (U $5f^3$). The CASSCF(3,7) relative energies of the lowest U $5f^3$ states for all the compounds are presented in the supporting information (Table S10). The energy profile for the quartet states shows three distinct energy gaps, one after state 13, one after state 21 and one after state 30. The lowest 13 quartets, (Set 1) separated by 7000 cm^{-1} (0.87 eV) from the higher ones, were further modeled with the MS-CASPT2 method. We also performed a second set of MS-CASPT2 calculations in which the first 21 quartets and 11 doublets were included (Set 2), i.e., including the next higher-energy block of quartets. The results of the MS-CASPT2 calculations are reported in Table S10. The results (energies and wave functions) from CASSCF(3,7) and MS-CASPT2(3,7) (sets 1 and 2) were used, in three independent sets of calculations, to obtain the spin-orbit coupled states and energies.

Table 2 shows the relative energies including spin-orbit (SO) coupling effects for compound **1**. We focus the discussion on the lowest 12 spin-orbit states. These states arise from the coupling of several states computed prior to the spin-orbit coupling. At both the CASSCF and MS-CASPT2 levels, the largest contribution (more than 93%) comes from the lowest 13 quartets and the second most important contribution (up to 6%) arises from the lowest 11 doublets (See Table S11). The first energy gap for SO-CASSCF(3,7) (108.7 cm^{-1}) is about half of that obtained from SO-MS-CASPT2(3,7) (181.0 and 199.3 cm^{-1}). The two CASPT2 values are in better agreement with previous results obtained from a crystal field model Hamiltonian (230 cm^{-1}), which was constructed from fitting magnetic susceptibility curves.³¹ Finally, comparing the two SO-MS-CASPT2(3,7) results, we notice that the inclusion of doublet states (set 2) affects the energies of

the lowest Kramer doublets, even though the largest contributions came from quartet states (See Table S11).

Table 2: Relative energies for the lowest Kramer doublets (cm^{-1}) for compound **1**. Spin-Orbit (SO) effects were included on top of CASSCF(3,7) and MS-CASPT2(3,7) (Set 1 and Set 2) energies.

Spin-orbit States	CASSCF	Set 1	Set 2
1-2	0.0	0.0	0.0
3-4	108.7	181.0	199.3
5-6	352.6	409.1	290.0
7-8	467.8	549.7	353.3
9-10	565.8	710.5	465.2
11-12	3743.7	3370.1	4391.1

Figure 3 presents the calculated magnetic susceptibility values, obtained according to eq. (1), for different methods together with the experimental data. The results obtained with the SO-CASSCF(3,7) energies are in good agreement with the experimental values at low temperature ($T < 100\text{K}$), but start to deviate more in the higher temperature regime ($T > 150\text{K}$). The low temperature magnetic susceptibility is dominated by the contribution from the lowest spin-orbit state (1-2), 95% at 50K and 82% at 100K based on the Boltzmann population (See Table S12). The magnetic moments (μ) of such states are independent of the temperature, a phenomenon called temperature independent paramagnetism (TIP), which means that the χT values are linear with temperature. This effect is observed in the experimental data below 50 K, and it is reproduced in all the computed curves. When the next spin-orbit states (3-4) start to increase their Boltzmann populations (4% at 50K and 17% at 100K), the shape of the χT curve changes. These excited states have a smaller μ compared to states 1-2, and so at higher temperatures the magnetic susceptibility averaged over the various contributing spin-orbit states (states 1 to 10

have 100% Boltzmann population at 300K) has a much smaller slope of χT . Ultimately, χT should plateau towards the free ion value, where the high temperature populates most of the states and the ligand field splitting is negligible. This can be seen for the experimental curve but not for the computed χT . Overall the SO-CASSCF(3,7) calculations correctly capture the magnetic behavior of the lowest energy states but underestimate the effect of the higher energy states.

The results from SO-MS-CASPT2(3,7) produce a curve that is shifted to higher values of χT and has a smaller slope at $T < 100\text{K}$ compared to SO-CASSCF(3,7) and experiment. This behavior was observed before in a different uranium SMM complex, and could be corrected for by applying an arbitrary factor to the calculated χT values.³² However, while such an empirical correction can provide agreement with experiment for a single case, it is unlikely to be transferable from one species to the other. Moreover, the high computational cost of the SO-MS-CASPT2(3,7) method makes it a challenge to apply to larger systems. Based on these results, we conclude that the formally less complete but computationally more practical SO-CASSCF(3,7) model is more suited for the examination of trends across systems, possibly owing to a fortuitous cancellation of errors, although SO-MS-CASPT2(3,7) might be preferable for the most accurate energetics in individual systems, when it is affordable.

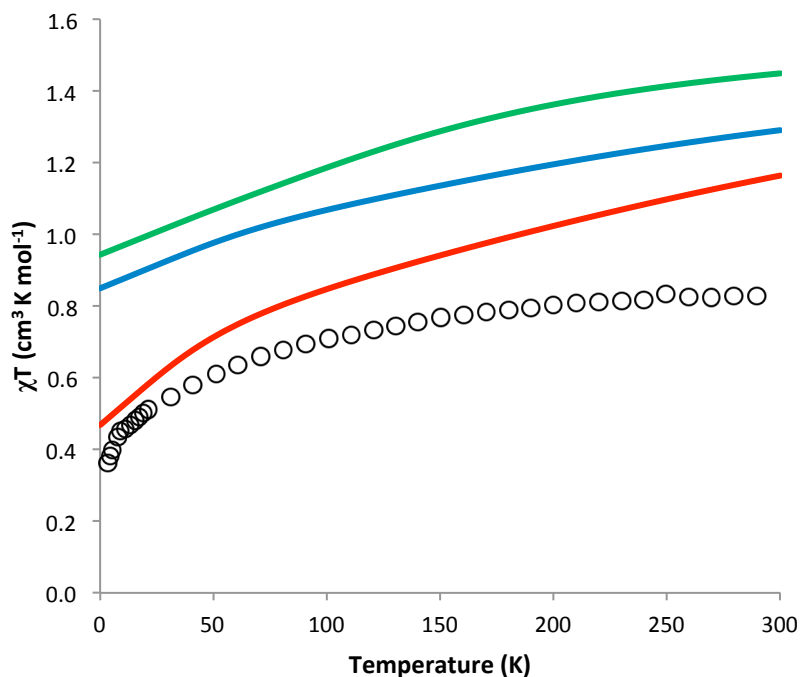


Figure 3: Magnetic susceptibility plot for compound **1**. Experiment (circles),¹⁶ SO-CASSCF (red) and SO-MS-CASPT2 (Set 1 blue, set 2 green).

We next calculated the magnetic susceptibility curves of compounds **2**, **3** and **4** using the more efficient SO-CASSCF(3,7) level of theory (Figure 4). The agreement between the SO-CASSCF(3,7) results and experiment is better for **2-4** than for **1**, and particularly good for **2**. Unlike for **1**, the calculated SO-CASSCF(3,7) curves for **2-4** lie below their experimental counterparts at higher temperature. Trends between compounds **2** and **3** are reasonably well reproduced, although with predicted differences smaller than measured. The magnetic susceptibility at very low temperatures ($T < 10\text{K}$) is higher for **2**, but the slope of the susceptibility is larger for **3** (Figure 4, inset). For $T > 30\text{K}$, the susceptibility of **3** is greater than that for **2** until approximately $T = 300\text{K}$ at which point the two values are comparable. Compounds **2** and **3** differ in coordinating either a nitrogen or a carbon atom to the metal. Experimentally, it has been

shown that the organometallic case **3** possesses slower magnetic relaxation with one of the highest effective barriers ($U_{\text{eff}} = 23 \text{ cm}^{-1}$) observed for a mono-uranium SMM; the coordination compound **2** does not show the same behavior.¹⁷ Their different relaxation behavior may be attributable to a magnetic anisotropy difference.

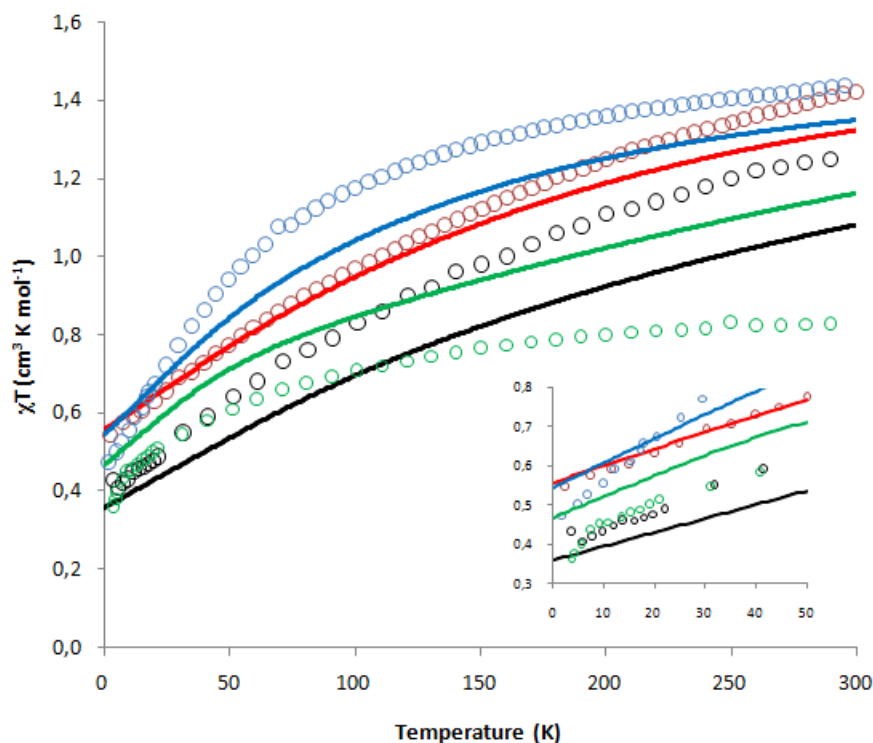


Figure 4: Magnetic susceptibility plot for compounds **1** (green), **2** (red), **3** (blue) and **4** (black). Experiment (circles)¹⁶⁻¹⁸ and SO-CASSCF(3,7) (lines). Inset shows the low temperature region.

Table 3: Relative Spin-Orbit CASSCF(3,7) energies for the lowest Kramer doublets (cm^{-1}) for compounds **1**, **2**, **3** and **4**. Experimental values for compound **4** in parenthesis.³⁰

Spin-orbit States	1	2	3	4	
1-2	0.0	0.0	0.0	0.0	(0.0)
3-4	108.7	174.7	109.0	257.9	(270)
5-6	352.6	394.3	322.1	607.2	-
7-8	467.8	502.7	403.9	1137.1	-
9-10	565.8	552.6	455.7	1185.6	-
11-12	3743.7	4482.7	4248.7	4665.4	(4354)

The relative energies for the calculated SO-CASSCF(3,7) states are presented in Table 3. The first energy gap between the Kramer doublets varies among the studied compounds. We also compare the values for compound **4** with the available experimental absorption data. The calculated energy gaps (257.9 and 4665.4 cm^{-1}) are in quite good agreement with the first two experimental peaks (270 and 4354 cm^{-1} , respectively).³⁰ This agreement for species **4** increases confidence in the computed results for compounds **2** and **3**. We attempt to correlate these excitation energies with the measured effective relaxation barriers (U_{eff}), although previous studies have not suggested any connection between these two quantities.³¹ The compounds with the largest experimental U_{eff} are **1** and **3** (16 and 23 cm^{-1} respectively), and our calculations show that these compounds have the lowest first energy gaps (108.7 and 109.0 cm^{-1}). This might suggest that these two compounds have similar relaxation processes, because they share similar excitation energies. More experimental evidence will be needed to assess further this relationship between state-energy separations and effective relaxation barriers.

IV. DISCUSSION

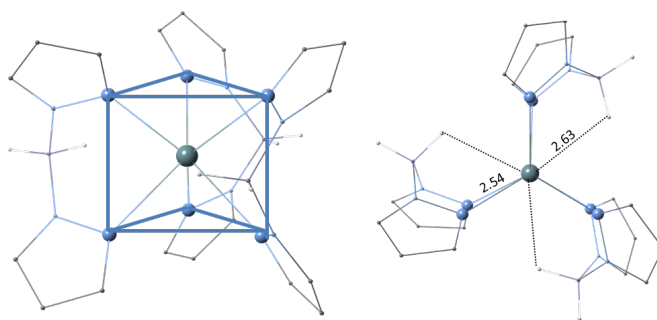


Figure 5: Schematic representation of compound **1** with side (left) and top (right) view of the tricapped trigonal prism.

All of the compounds examined here have a tricapped trigonal prismatic coordination geometry around the uranium (Figure 5), consisting of six N (or C) and three extra residues in an equatorial position at a slightly larger distance. For compounds **1**, **2** and **3**, the residues consist of a H directly bonded to the B in the borate ligand (see left side of Figure 5), whereas **4** has the extra pyrazolyl rings of the Tp₃ ligand. In the case of **1**, the agostic interaction between H and the uranium have been suggested to play an important role in the magnetic properties of the compound, particularly when compared to the phenyl substituted boron derivate (U(Ph₂BPz₂)₃) of **1**, which lacks the U-H interaction.⁶ The presence of the equatorial interaction axially elongates the prism, increasing the U-N (or C) distances. Table 4 presents the most relevant geometrical parameters of the studied compounds (experimental structures of **1**, **2** and **3**, BP86/TZ2P optimized geometry of **4**) and the Mulliken charges of the uranium centers obtained from the CASSCF wave function of the ground state.

Table 4: Geometric parameters and partial atomic charges (at CASSCF level) for the studied compounds. L is nitrogen except for compound **3** (carbon). R is hydrogen except for compound **4** (nitrogen).

Compound	U-L (Å)	U-R (Å)	Bite Angle	$q(\text{U}^{3+})$	U_{eff} (cm-1)	dE_{calc} (cm ⁻¹)
1	2.535	2.856	78.9	1.35	16	108.7
2	2.588	2.626	76.7	1.50	-	174.7
3	2.661	2.750	73.8	0.81	23	109.0
4	2.583	2.781	77.1	1.76	3.8	257.9

Taking into account that all the ligands act as σ -donors, a stronger ligand interaction with uranium would mean a higher electron donation towards the uranium and a smaller positive charge on the latter. The Mulliken charges suggest that compound **3** has the largest electron donation to the uranium center (through covalency), followed by compounds **1**, **2** and **4**. Thus,

the ligand field strength should follow the same trend, and this has been confirmed in a qualitative manner, by the ligand field splitting of the U 5f orbitals at DFT/BP86 level.

The differences between **1** and **2** can be attributed to elongation of the U-N distances (from 2.535 to 2.588 Å) that weaken the ligand-uranium interaction in the latter. This elongation could be the result of steric repulsion between the substituted methyl groups that point towards the pyrazolyl rings of the other close ligands. In a similar fashion, compound **4** has the extra pyrazolyl on the boron center facing towards the other ligands, and the bulky substituents force longer distances to the uranium center, which lead to the weakest ligand field.

The stronger interaction depicted in **3** can be attributed to the higher basicity and greater covalency of the carbene ligand, compared to pyrazolyl in **2**, which outweighs that the distance between the ligand and the uranium is longer in **3** than in **2** (2.661 vs 2.588 Å, respectively).

We identify compounds **1** and **3** as the best performing single molecule magnets, due to their effective barriers for magnetic relaxation. Both compounds have a similar energy separation for their lowest spin-orbit states and we have computed that they also have the strongest ligand fields.

With this in mind, we studied a hypothetical isomer of **4**, with C instead of N bonded to the uranium (i.e., incorporating carbene-like ligands, which we label as **4'**). The optimized structure of **4'** with DFT/BP86 confirms trends noted above: an elongation of the distance between uranium and the ligands (from 2.583 to 2.635 Å) and a larger splitting of the U 5f orbitals. In addition, SO-CASSCF(3,7) results indicate a smaller Mulliken U charge (1.17 compared to 1.76 of **4**) and lower energy separation for the first excited spin-orbit states (58.8 cm⁻¹). For the complete results see the supporting information.

From this computational experiment we conclude that carbene ligands could help to generate compounds with larger ligand-field splittings. It is important to note that in the experimental carbene compound (**3**), the ligand contains a methyl group substituting the alpha nitrogen. This could be important in two respects: it could stabilize the carbene structure by blocking the nitrogen as a donor center, and it may influence the interaction with the metal by the elongation of the distance due to steric repulsion. Therefore, the substituting group could be key to modulating the proper ligand field to obtain good magnetic properties.

V. CONCLUSIONS

Multiconfigurational electronic structure theory calculations for four uranium-based single-molecule-magnets indicate that consideration of uranium $5f^3$ states alone is sufficient to account for all energetically relevant spin-orbit coupling effects. Trends in experimental magnetic susceptibility curves were well reproduced when considering all possible quartets and doublets with a spin-orbit CASSCF model including 3 electrons in 7 ($5f$) orbitals. For **4**, calculated energy gaps between spin-orbit states agreed well with the first two peaks of the experimental absorption spectrum. In addition to expanding our understanding of the electronic structure and magnetic behaviour of uranium SMMs, we anticipate that analogous modeling will prove useful for the study of trans-uranium SMMs.

VI. ASSOCIATED CONTENT

Supporting Information. Experimental and computed structures details are reported, with associated energies. This material is available free of charge via the Internet at <http://pubs.acs.org>.

VII. AUTHOR INFORMATION

Corresponding Authors

*cramer@umn.edu; @ChemProfCramer (CJC)

*gagliard@umn.edu (LG)

VIII. ACKNOWLEDGMENTS

This work was supported by the Division of Chemical Sciences, Geosciences, and Biosciences, Office of Basic Energy Sciences of the U.S. Department of Energy under grant n. USDOE/DESC002183 (K.D.V., M.S. and L.G.), U.S. Department of Energy, Office of Science, Office of Advanced Scientific Computing Research, Scientific Discovery through Advanced Computing (SciDAC) program under Award Number DE-SC0008666.(C.J.C.), the Spanish Administration under project CTQ2014-51938-P and the Generalitat de Catalunya under project 2014SGR199 (M.S and C.deG.)

REFERENCES

1. R. Sessoli, H. L. T., A. R. Schake, S. Wang, J. B. Vincent, K. Folting, D. Gatteschi, G. Christou, and D. N. Hendrickson, High-spin molecules: $[\text{Mn}_{12}\text{O}_{12}(\text{O}_2\text{CR})_{16}(\text{H}_2\text{O})_4]$. *Journal of the American Chemical Society* **1993**, 115.
2. (a) S. M. J. Aubin, M. W. W., D. M. Adams, H.-L. Tsai, G. Christou, and D. N. Hendrickson, Distorted MnIVMnIII_3 Cubane Complexes as Single-Molecule Magnets. *Journal of the American Chemical Society* **1996**, 118; (b) S. M. J. Aubin, Z. S., L. Pardi, J. Krzystek, K. Folting, L.-C. Brunel, A. L. Rheingold, G. Christou, and D. N. Hendrickson, Reduced Anionic Mn_{12} Molecules with Half-Integer Ground States as Single-Molecule Magnets. *Inorganic Chemistry* **1999**, 38.
3. (a) Aromí, G.; Brechin, E. K., Synthesis of 3d Metallic Single-Molecule Magnets. In *Single-Molecule Magnets and Related Phenomena*, Winpenny, R., Ed. Springer Berlin Heidelberg: Berlin, Heidelberg, 2006; pp 1-67; (b) Rinehart, J. D.; Harris, T. D.; Kozimor, S. A.;

Bartlett, B. M.; Long, J. R., Magnetic Exchange Coupling in Actinide-Containing Molecules. *Inorganic Chemistry* **2009**, *48* (8), 3382-3395.

4. (a) Sessoli, R.; Powell, A. K., Strategies towards single molecule magnets based on lanthanide ions. *Coordination Chemistry Reviews* **2009**, *253* (19–20), 2328-2341; (b) Lin, P.-H.; Burchell, T. J.; Ungur, L.; Chibotaru, L. F.; Wernsdorfer, W.; Murugesu, M., A Polynuclear Lanthanide Single-Molecule Magnet with a Record Anisotropic Barrier. *Angewandte Chemie International Edition* **2009**, *48* (50), 9489-9492; (c) Ishikawa, N.; Sugita, M.; Wernsdorfer, W., Quantum Tunneling of Magnetization in Lanthanide Single-Molecule Magnets: Bis(phthalocyaninato)terbium and Bis(phthalocyaninato)dysprosium Anions. *Angewandte Chemie International Edition* **2005**, *44* (19), 2931-2935; (d) Layfield, R. A.; McDouall, J. J. W.; Sulway, S. A.; Tuna, F.; Collison, D.; Winpenny, R. E. P., Influence of the N-Bridging Ligand on Magnetic Relaxation in an Organometallic Dysprosium Single-Molecule Magnet. *Chemistry – A European Journal* **2010**, *16* (15), 4442-4446.

5. Newell, B. S.; Rappé, A. K.; Shores, M. P., Experimental Evidence for Magnetic Exchange in Di- and Trinuclear Uranium(IV) Ethynylbenzene Complexes. *Inorganic Chemistry* **2010**, *49* (4), 1595-1606.

6. Meihaus, K. R.; Long, J. R., Actinide-based single-molecule magnets. *Dalton Transactions* **2015**, *44* (6), 2517-2528.

7. (a) Mok, D. K. W.; Neumann, R.; Handy, N. C., Dynamical and nondynamical correlation. *Journal of Physical Chemistry* **1996**, *100* (15), 6225-6230; (b) Handy, N. C.; Cohen, A. J., Left-right correlation energy. *Molecular Physics* **2001**, *99* (5), 403-412; (c) Hollett, J. W.; Gill, P. M. W., The two faces of static correlation. *Journal of Chemical Physics* **2011**, *134* (11), 1141111.

8. (a) Schultz, N. E.; Zhao, Y.; Truhlar, D. G., Density functionals for inorganometallic and organometallic chemistry. *J. Phys. Chem. A* **2005**, *109* (49), 11127-11143; (b) Harvey, J. N., On the accuracy of density functional theory in transition metal chemistry. In *Annu. Rep. Prog. Chem. C*, 2006; Vol. 102(1), pp 203-226; (c) Cohen, A. J.; Mori-Sanchez, P.; Yang, W. T., Insights into current limitations of density functional theory. *Science* **2008**, *321* (5890), 792-794.

9. Roos, B. O.; Taylor, P. R.; Siegbahn, P. E. M., A Complete Active Space Scf Method (Casscf) Using a Density-Matrix Formulated Super-Ci Approach. *Chemical Physics* **1980**, *48* (2), 157-173.

10. (a) Andersson, K.; Malmqvist, P.-Å.; Roos, B. O., 2nd-order perturbation-theory with a complete active space self-consistent field reference function. *Journal of Chemical Physics* **1992**, *96* (2), 1218-1226; (b) Andersson, K.; Malmqvist, P. A.; Roos, B. O.; Sadlej, A. J.; Wolinski, K., Second-order perturbation theory with a CASSCF reference function. *The Journal of Physical Chemistry* **1990**, *94* (14), 5483-5488.

11. Siegbahn, P. E. M.; Almlöf, J.; Heiberg, A.; Roos, B. O., The complete active space scf (CASSCF) method in a Newton-Raphson formulation with application to the HNO molecule. *Journal of Chemical Physics* **1981**, *74* (4), 2384-2396.

12. (a) Malmqvist, P. A.; Rendell, A.; Roos, B. O., The restricted active space self-consistent-field method, implemented with a split graph unitary group approach. *The Journal of Physical Chemistry* **1990**, *94* (14), 5477-5482; (b) Malmqvist, P. Å.; Pierloot, K.; Shahi, A. R. M.; Cramer, C. J.; Gagliardi, L., The restricted active space followed by second-order perturbation theory method: Theory and application to the study of CuO₂ and Cu₂O₂ systems. *Journal of Chemical Physics* **2008**, *128* (20), 204109.

13. (a) Ma, D.; Li Manni, G.; Gagliardi, L., The Generalized Active Space concept in Multiconfigurational Self-Consistent-Field methods. *Journal of Chemical Physics* **2011**, *135* (4), 044128 ; (b) Olsen, J.; Roos, B. O.; Jorgensen, P.; Jensen, H. J. A., Determinant based Configuration-Interaction algorithms for complete and restricted Configuration-Interaction spaces. *Journal of Chemical Physics* **1988**, *89* (4), 2185-2192; (c) Fleig, T.; Olsen, J.; Marian, C. M., The generalized active space concept for the relativistic treatment of electron correlation. I. Kramers-restricted two-component configuration interaction. *Journal of Chemical Physics* **2001**, *114* (11), 4775-4790; (d) Ma, D. X.; Manni, G. L.; Olsen, J.; Gagliardi, L., Second-Order Perturbation Theory for Generalized Active Space Self Consistent-Field Wave Functions. *J. Chem. Theory Comput.* **2016**, *12* (7), 3208-3213.
14. (a) Ivanic, J., Direct configuration interaction and multiconfigurational self-consistent-field method for multiple active spaces with variable occupations. I. Method. *Journal of Chemical Physics* **2003**, *119* (18), 9364-9376; (b) Ivanic, J.; Ruedenberg, K., Identification of deadwood in configuration spaces through general direct configuration interaction. *Theor. Chem. Acc.* **2001**, *106* (5), 339-351.
15. (a) Chibotaru, L. F.; Ungur, L., Ab initio calculation of anisotropic magnetic properties of complexes. I. Unique definition of pseudospin Hamiltonians and their derivation. *The Journal of Chemical Physics* **2012**, *137* (6), 064112; (b) Gendron, F.; Pritchard, B.; Bolvin, H.; Autschbach, J., Single-ion 4f element magnetism: an ab-initio look at Ln(COT)₂. *Dalton Transactions* **2015**, *44* (46), 19886-19900.
16. Rinehart, J. D.; Meihaus, K. R.; Long, J. R., Observation of a Secondary Slow Relaxation Process for the Field-Induced Single-Molecule Magnet U(H₂BPz₂)₃. *Journal of the American Chemical Society* **2010**, *132* (22), 7572-7573.
17. Meihaus, K. R.; Minasian, S. G.; Lukens, W. W.; Kozimor, S. A.; Shuh, D. K.; Tylliszczak, T.; Long, J. R., Influence of Pyrazolate vs N-Heterocyclic Carbene Ligands on the Slow Magnetic Relaxation of Homoleptic Trischelate Lanthanide(III) and Uranium(III) Complexes. *Journal of the American Chemical Society* **2014**, *136* (16), 6056-6068.
18. Rinehart, J. D.; Long, J. R., Slow magnetic relaxation in homoleptic trispyrazolylborate complexes of neodymium(iii) and uranium(iii). *Dalton Transactions* **2012**, *41* (44), 13572-13574.
19. Aquilante, F.; Autschbach, J.; Carlson, R. K.; Chibotaru, L. F.; Delcey, M. G.; De Vico, L.; Fdez. Galván, I.; Ferré, N.; Frutos, L. M.; Gagliardi, L.; Garavelli, M.; Giussani, A.; Hoyer, C. E.; Li Manni, G.; Lischka, H.; Ma, D.; Malmqvist, P. Å.; Müller, T.; Nenov, A.; Olivucci, M.; Pedersen, T. B.; Peng, D.; Plasser, F.; Pritchard, B.; Reiher, M.; Rivalta, I.; Schapiro, I.; Segarra-Martí, J.; Stenrup, M.; Truhlar, D. G.; Ungur, L.; Valentini, A.; Vancoillie, S.; Veryazov, V.; Vysotskiy, V. P.; Weingart, O.; Zapata, F.; Lindh, R., Molcas 8: New capabilities for multiconfigurational quantum chemical calculations across the periodic table. *Journal of Computational Chemistry* **2016**, *37* (5), 506-541.
20. Roos, O. B.; Veryazov, V.; Widmark, P.-O., Relativistic atomic natural orbital type basis sets for the alkaline and alkaline-earth atoms applied to the ground-state potentials for the corresponding dimers. *Theor. Chem. Acc.* **2004**, *111* (2), 345-351.
21. Wolf, A.; Reiher, M.; Hess, B. A., The generalized Douglas-Kroll transformation. *The Journal of Chemical Physics* **2002**, *117* (20), 9215-9226.
22. Aquilante, F.; Malmqvist, P.-Å.; Pedersen, T. B.; Ghosh, A.; Roos, B. O., Cholesky Decomposition-Based Multiconfiguration Second-Order Perturbation Theory (CD-CASPT2):

Application to the Spin-State Energetics of CoIII(diiminato)(NPh). *J. Chem. Theory Comput.* **2008**, *4* (5), 694-702.

23. Malmqvist, P. Å.; Roos, B. O.; Schimmelpfennig, B., The restricted active space (RAS) state interaction approach with spin-orbit coupling. *Chemical Physics Letters* **2002**, *357* (3-4), 230-240.

24. (a) Chibotaru, L. F.; Ungur, L.; Soncini, A., The Origin of Nonmagnetic Kramers Doublets in the Ground State of Dysprosium Triangles: Evidence for a Toroidal Magnetic Moment. *Angewandte Chemie International Edition* **2008**, *47* (22), 4126-4129; (b) Chibotaru, L. F.; Ungur, L.; Aronica, C.; Elmoll, H.; Pilet, G.; Luneau, D., Structure, Magnetism, and Theoretical Study of a Mixed-Valence CoII3CoIII4 Heptanuclear Wheel: Lack of SMM Behavior despite Negative Magnetic Anisotropy. *Journal of the American Chemical Society* **2008**, *130* (37), 12445-12455; (c) Ungur, L.; Thewissen, M.; Costes, J.-P.; Wernsdorfer, W.; Chibotaru, L. F., Interplay of Strongly Anisotropic Metal Ions in Magnetic Blocking of Complexes. *Inorganic Chemistry* **2013**, *52* (11), 6328-6337.

25. Becke, A. D., Density-functional thermochemistry. IV. A new dynamical correlation functional and implications for exact-exchange mixing. *The Journal of Chemical Physics* **1996**, *104* (3), 1040-1046.

26. (a) Becke, A. D., Density-functional thermochemistry. III. The role of exact exchange. *The Journal of Chemical Physics* **1993**, *98* (7), 5648-5652; (b) Lee, C.; Yang, W.; Parr, R. G., Development of the Colle-Salvetti correlation-energy formula into a functional of the electron density. *Physical Review B* **1988**, *37* (2), 785-789.

27. Zhao, Y.; Truhlar, D. G., A new local density functional for main-group thermochemistry, transition metal bonding, thermochemical kinetics, and noncovalent interactions. *The Journal of Chemical Physics* **2006**, *125* (19), 194101.

28. Lenthe, E. v.; Baerends, E. J.; Snijders, J. G., Relativistic regular two-component Hamiltonians. *The Journal of Chemical Physics* **1993**, *99* (6), 4597-4610.

29. (a) Fonseca Guerra, C.; Snijders, G. J.; te Velde, G.; Baerends, J. E., Towards an order-N DFT method. *Theor. Chem. Acc.* **1998**, *99* (6), 391-403; (b) SCM Theoretical Chemistry, V. U., Amsterdam, The Netherlands <http://www.scm.com>. *ADF2013*; (c) te Velde, G.; Bickelhaupt, F. M.; Baerends, E. J.; Fonseca Guerra, C.; van Gisbergen, S. J. A.; Snijders, J. G.; Ziegler, T., Chemistry with ADF. *Journal of Computational Chemistry* **2001**, *22* (9), 931-967.

30. Apostolidis, C.; Morgenstern, A.; Rebizant, J.; Kanellakopoulos, B.; Walter, O.; Powietzka, B.; Karbowiak, M.; Reddmann, H.; Amberger, H.-D., Zur Elektronenstruktur hochsymmetrischer Verbindungen der f-Elemente 44 [1]. Erstmalige parametrische Analyse des Absorptionsspektrums einer Molekülverbindung des trivalenten Urans: Tris[hydrotris(1-pyrazolyl)borato]uran(III) Electronic Structures of Highly Symmetrical Compounds of f Elements 44 [1]. First Parametric Analysis of the Absorption Spectrum of a Molecular Compound of Tervalent Uranium: Tris[hydrotris(1-pyrazolyl)borato]uranium(III). *Zeitschrift für anorganische und allgemeine Chemie* **2010**, *636* (1), 201-208.

31. Baldovi, J. J.; Cardona-Serra, S.; Clemente-Juan, J. M.; Coronado, E.; Gaita-Arino, A., Modeling the properties of uranium-based single ion magnets. *Chemical Science* **2013**, *4* (3), 938-946.

32. Coutinho, J. T.; Antunes, M. A.; Pereira, L. C. J.; Bolvin, H.; Marcalo, J.; Mazzanti, M.; Almeida, M., Single-ion magnet behaviour in [U(TpMe2)2I]. *Dalton Transactions* **2012**, *41* (44), 13568-13571.

